



This is a repository copy of *Application of low frequency vibration to the turning of ultra-high molecular weight polyethylene.*

White Rose Research Online URL for this paper:

<https://eprints.whiterose.ac.uk/221667/>

Version: Published Version

Article:

Rooke, J. orcid.org/0000-0003-0720-7891, Bonnell, R. orcid.org/0009-0003-6531-5169, Pickford, E. orcid.org/0009-0008-5548-4723 et al. (2 more authors) (2025) Application of low frequency vibration to the turning of ultra-high molecular weight polyethylene. *Advanced Manufacturing: Polymer & Composites Science*, 11 (1). ISSN 2055-0340

<https://doi.org/10.1080/20550340.2025.2449631>

Reuse

This article is distributed under the terms of the Creative Commons Attribution (CC BY) licence. This licence allows you to distribute, remix, tweak, and build upon the work, even commercially, as long as you credit the authors for the original work. More information and the full terms of the licence here:

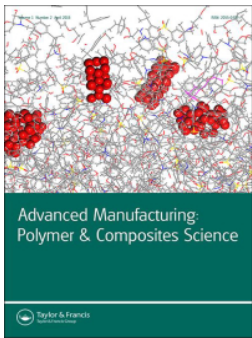
<https://creativecommons.org/licenses/>

Takedown

If you consider content in White Rose Research Online to be in breach of UK law, please notify us by emailing eprints@whiterose.ac.uk including the URL of the record and the reason for the withdrawal request.



eprints@whiterose.ac.uk
<https://eprints.whiterose.ac.uk/>



Application of low frequency vibration to the turning of ultra-high molecular weight polyethylene

Jack Rooke, Richard Bonnell, Emily Pickford, Adam Brown & David Curtis

To cite this article: Jack Rooke, Richard Bonnell, Emily Pickford, Adam Brown & David Curtis (2025) Application of low frequency vibration to the turning of ultra-high molecular weight polyethylene, *Advanced Manufacturing: Polymer & Composites Science*, 11:1, 2449631, DOI: [10.1080/20550340.2025.2449631](https://doi.org/10.1080/20550340.2025.2449631)

To link to this article: <https://doi.org/10.1080/20550340.2025.2449631>



© 2025 The Author(s). Published by Informa UK Limited, trading as Taylor & Francis Group.



Published online: 10 Jan 2025.



Submit your article to this journal [↗](#)



Article views: 6



View related articles [↗](#)



View Crossmark data [↗](#)

Application of low frequency vibration to the turning of ultra-high molecular weight polyethylene

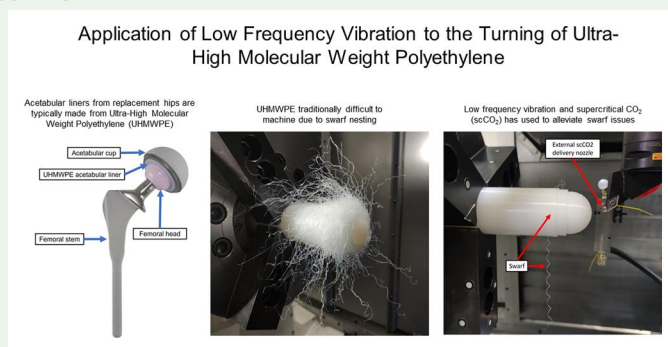
Jack Rooke , Richard Bonnell , Emily Pickford , Adam Brown  and David Curtis 

Advanced Manufacturing Research Centre, University of Sheffield, Rotherham, UK

ABSTRACT

Medical implant manufacturing is a growing sector and therefore requires improved manufacturing practices. In the case of total hip arthroplasty, the most challenging component to meet the ISO standard (ISO 7206-2:2011) is the acetabular liner, often made from ultra-high molecular weight polyethylene (UHMWPE). UHMWPE machining is associated with several manufacturing challenges, including swarf control. This research used low frequency vibration (LFV), an intermittent cutting process and supercritical CO₂ (scCO₂) to aid chip segmentation and prevent swarf nesting. Machining trials have demonstrated a significant reduction in swarf nesting relative to a traditional process (91% reduction from LFV and 98% reduction when using LFV and scCO₂). The surface roughness (*Ra_Symbol*) also had an indirect improvement from using LFV (53% reduction on the inner hemisphere), leading to all parts meeting the roughness requirement of ISO 7206-2:2011. The results have demonstrated machinability benefits for UHMWPE, reducing the operator intervention required and component scrap rates.

GRAPHICAL ABSTRACT



ARTICLE HISTORY

Received 31 October 2024
Accepted 24 December 2024

KEYWORDS

Ultra-high molecular weight polyethylene; UHMWPE; low frequency vibration; swarf chipping

1. Introduction

Total hip arthroplasty is a growing sector, fed by an ageing population and increasing prevalence of obesity in western countries. Therefore, globally, the total number of hip arthroplasty operations has surpassed one million annually [1], with the OCED countries averaging 174 hip replacement surgeries per 100,000 in 2019 [2]. Based on the volume of operations in the United States in 2019, Shichman et al. [3] projected that the number of total hip arthroplasty procedures will increase by 176% by 2040 and 659% by 2060. Therefore, improved manufacturing practices are required to meet the demand for a greater number of procedures and increased component customisation.

The components comprising a typical hip replacement are shown in Figure 1.

The main cause of hip implant failure is osteolysis, which is induced by ultra-high molecular weight polyethylene (UHMWPE) wear particles. The wear rate of UHMWPE is increased from inappropriate dimensional parameters and surface finish between the acetabular liner and femoral head tribological pair [5]. Cubillos et al. [6] have previously reviewed a series of acetabular liner and femoral head manufacturers against the relevant ISO standard (ISO 7206-2:2011) to assess the manufacturers' conformance. The research found that the femoral heads met the standards whilst the acetabular liners often did not. Of the five manufacturers, two did not

CONTACT Jack Rooke  jack.rooke@amrc.co.uk  Advanced Manufacturing Research Centre, University of Sheffield, Rotherham, South Yorkshire, UK

© 2025 The Author(s). Published by Informa UK Limited, trading as Taylor & Francis Group.

This is an Open Access article distributed under the terms of the Creative Commons Attribution License (<http://creativecommons.org/licenses/by/4.0/>), which permits unrestricted use, distribution, and reproduction in any medium, provided the original work is properly cited. The terms on which this article has been published allow the posting of the Accepted Manuscript in a repository by the author(s) or with their consent.

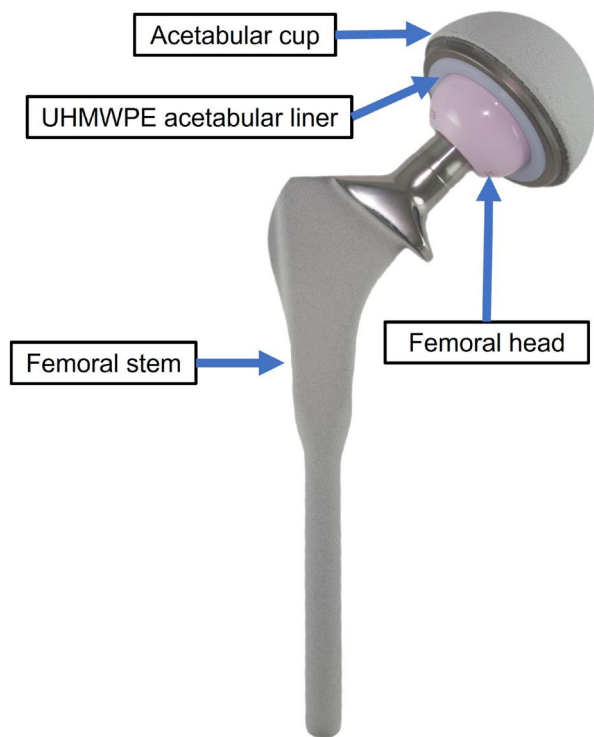


Figure 1. Hip replacement components. The implant shown is a furlong HAC stem, ceramic head and UHMWPE liner. Image edited from that provided by JRI orthopaedics [4].

meet the diameter tolerances, one did not meet the surface finish requirements ($R_{a_{max}}$ below $2 \mu m$) and a significant variation in the sphericity $37 \pm 17 \mu m$ was also measured. It is also worth noting that each of the acetabular liner manufacturers struggled to adhere to different areas of the ISO standard, implying that the manufacturing issues are not inherently due to the material, rather than the manufacturing process used.

Polymers such as UHMWPE are often used in medical applications due to their customisable properties, which enable biocompatibility, a low coefficient of friction (UHMWPE has a lower coefficient of friction than other similar polymers) and their mechanical performance [7,8]. Due to these properties, UHMWPE is used in a range of biomedical applications: knee, hip, ankle, shoulder, elbow, spinal, and finger, however, this research focuses on the total hip arthroplasty case study. A drawback of using a polymer is that the polymer will more readily wear than an equivalent metallic component, leading to the release of wear debris into the body of the implant recipient [9,10]. However, polymer wear particles are preferential over metallic wear particles. Antioxidants such as Vitamin E are often used to improve the wear characteristics of UHMWPE [11,12]. Alternatively, UHMWPE can be cross-linked to further reduce the wear rate. Tsukamoto et al. [13] studied the wear rate of 7-Mrad UHMWPE with a zirconia femoral condyle, and after 5.5 million cycles no measurable wear was observed.

Polymer machining has several additional complexities beyond those of machining metallics [14], such as low thermal conductivity, viscoelastic behaviour, glass transition temperature (T_g) and chip formation. For example, polymers have previously been shown to have six different types of chip morphology [15] depending on the machining parameters. In addition, parameters such as the sharpness of the tool have an impact on the surface deformation of the polymer and the effective depth of cut due to the material's elastic recovery and viscous relaxation [16]. Furthermore, due to the medical application, the polymer is often machined dry or with a biocompatible coolant to prevent contamination from an oil-based metal-working fluid.

The machining of UHMWPE commonly leads to burr generation, Aldwell et al. [17] have suggested that the increased temperature in the cutting zone (polymers have a low thermal conductivity) increases the workpiece deformation and leads to the generation of burrs. Due to this, UHMWPE and similar polymers have been machined using hybrid processes, in which the material is cooled to raise its stiffness. It has been shown that machining above, but close to, the T_g of the material can improve the surface quality of the machined polymer [18] whilst machining below the T_g changes the material to a glass-like state further raising the stiffness. This has led to polymers often being machined with the addition of cryogenics [17–23]. The glass transition temperature of UHMWPE varies depending on source with the majority falling between $-110^\circ C$ and $-160^\circ C$ [11, 16, 20, 24] with a significant outlier from Kustandi et al. [25] of $-26^\circ C$. The outlier T_g was determined using a differential scanning calorimetry. Applying cryogenic cooling to UHMWPE machining has, in general, been found to improve the surface finish. In the case of Bertolini et al. [20], a thermocouple was located 1 mm from the cutting zone with a liquid nitrogen coolant. The thermocouple measured $-50^\circ C$; therefore, it is expected that the cutting zone was above the T_g . Suggesting that the machinability of UHMWPE may be improved by a cryogenic coolant, even if the material is above its glass transition temperature and, therefore, in its ductile region. One application of cryogenics in the machining of polymers (PP, PE and PEEK) used dry ice to assist in deburring plastic parts [26]. Takumi [26] used the system developed by Cold Jet [27] to deburr parts post-machining. It is worth noting that the cryogenic cooling discussed here, excluding Takumi [26], is not on real-world components but a lab-based test piece devoid of real-world manufacturing complexities and their applicability to real-world components may be limited.

Machining polymers such as UHMWPE may be difficult due to the polymer itself being the least rigid component in the manufacturing environment. Therefore, the polymer is liable to deflect when it is in contact with the tool [28] leading to a variation in the effective depth of cut. Several further issues are prevalent when specifically machining UHMWPE; swarf nests around the part/tool, burr generation and part distortion/plastic relaxation. UHMWPE swarf nests around the bar/tool during each operation due to difficulty in causing the material to chip. The swarf nesting can also impact the cutting process by varying the effective depth of cut and if the swarf melts to the part/insert it will deteriorate the surface finish. In industry, this is often an accepted consequence of machining UHMWPE and is merely managed by the machine tool operator manually removing the swarf after each operation, limiting productivity and undoubtedly leading to a greater scrap rate. The generation of burrs when machining UHMWPE is typically managed by developing a process that pushes the burrs to a desired edge and the burr is removed in a post-machining operation. Finally, part distortion is a concern due to polymer relaxation post-machining and the relatively large thermal expansion of UHMWPE, therefore, the increased temperature in the cutting zone leads to localised expansion, varying the effective depth of cut. The distortion may also be managed by the addition of a coolant; however, if an oil-based coolant is used then there will be a greater cleaning requirement because of the medical application. This article focuses on alleviating the issue of swarf nesting around the part/tool and is applied to the case study of a UHMWPE acetabular liner.

A potential route to alleviate swarf nesting is through vibration assistance. This could either be done at low frequencies (Low Frequency Vibration (LFV)) or high frequencies (Ultrasonically Assisted Vibration). Neither vibration assistance has been applied to the machining of UHMWPE for medical components and therefore both may prove beneficial. However, lower frequency vibration more readily enables greater amplitudes of vibration in a typical machine tool and a greater amplitude of vibration will likely aid in swarf chipping. Therefore, LFV is considered in this article, although further research is required to determine the potential benefits of implementing ultrasonically assisted vibration.

LFV is an intermittent turning process that oscillates the insert in the feed direction. This, therefore, dictates the time-in-cut and chip length (see Figure 2), which means that the toolpath is the driving force for chip breaking and negates the

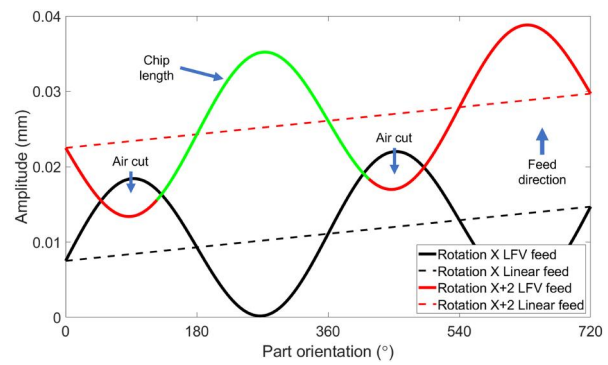


Figure 2. Linear feed versus low frequency vibration (LFV) feed.

need for other chip-breaking methods. The amplitude of LFV is typically in the order of 20–30 μm with a frequency of up to 1 kHz (lower frequencies than would be used in ultrasonically assisted vibration). The oscillating action of the tool relative to the workpiece leads to an irregular cutting face geometry which is removed by the tool not oscillating on the final rotation of the workpiece. In addition, there is a phase change of the oscillation in sequential rotations of the workpiece which leads to the phase of the air cut changing in each rotation. This intermittent cutting process essentially leads to the feedrate doubling and halving at different stages of each cutting cycle leading to a general recommendation to half the feedrate if using LFV. A detailed summary of the physics behind LFV and its implementation can be found in Nakamura et al. [29].

LFV has been applied in the machining of metallics [30,31] and plastic components [32–34]. The tool vibration methodology has shown success in terms of swarf control and provides other benefits such as removal of built-up edge, improved tool life, and machining temperature reduction/stability. However, this vibration technique has not previously been applied to the machining of UHMWPE.

A key consideration in the medical industry is the cleanliness of the components. UHMWPE is often machined dry, however, in this machining trial, supercritical CO₂ (scCO₂) was supplied using the PureCut system produced by Fusion Coolant Systems [27]. This solution enables scCO₂ and scCO₂ mixed with minimum quantity lubrication, delivered either through spindle or *via* an external nozzle. Supercritical CO₂ can be considered a clean coolant as the CO₂ evaporates from the surface and it negates the need for a traditional oil-based coolant. Using a clean coolant may also reduce the need for an extensive cleaning process post-machining. Using carbon dioxide for a coolant also has reported benefits such as improved chip breakability [35], improved surface finish [17, 20], reduced machining temperature, friction reduction

[35,36], and improved tool life [37]. Furthermore, cryogenic machining is an approach that meets the three pillars of sustainable machining (environmental, societal and economical) [38] and excludes several complications from conventional metalworking fluids (environmental pollution, water pollution and biological pollution). A sustainable and green scCO₂ delivery system could be achieved from a closed loop system to capture the expelled CO₂. Lu et al. [39] conducted a comparison between cryogenic and conventional metalworking fluids and found that cryogenic coolants had close to a 50% reduction in greenhouse gases emitted and a 26% reduction in total costs per part. An additional consideration with the application of cryogenic coolants in polymer machining is the contraction rate of the polymer (or reduction of thermal expansion). In Dhokia et al. [40], the contraction rate of ethylene vinyl acetate was determined and used to scale the CAM model. The research found the model was within 1% of the measured contraction, therefore, it may be plausible to account for UHMWPE contraction. Several review articles have been written concerning cryogenic coolants, the author highlights Proud et al. [41], Sivarupan et al. [37] and Khanna et al. [35] for an in-depth review.

In summary, the machining of UHMWPE is fraught with issues, predominately relating to swarf management, burr generation and part distortion/plastic relaxation. This article explores how to improve UHMWPE swarf management through the implementation of LFV, a vibration assistance methodology which has seen benefits in both metallic and polymer machining. Furthermore, the machinability of several polymers has previously been shown to improve when cryogenic coolants have been applied; however, this was typically applied to simplistic toolpaths/at low technology readiness levels. In this research, scCO₂ has been used in the machining of a part that is representative of a real-world component, in a representative machining process. Furthermore, as the case study is from the medical sector, it emphasises the potential benefit of implementing a clean coolant.

2. Experimental methodology

The experimental trials were conducted on a DMG MORI NTX 2500, a five-axis, mill-turn machine with two workpiece spindles. To produce industrially representative acetabular liners the outer hemisphere was machined in the main spindle before being parted off/transferred to the sub-spindle to complete the manufacturing process.

A software retrofit was performed on the NTX 2500 to enable LFV implementation, which is

controlled by defining two parameters, the amplitude magnification (K) and the number of cycles per rotation of the spindle (I). Initially, the first roughing operation (outer hemisphere roughing) was the focus of LFV implementation, and this was machined in the main spindle which had a maximum rotational speed of 3000 rpm. When LFV is typically used on hemispheres, the magnification factor is between 1.2–2 and I is limited by the maximum oscillation frequency, see Equation (1). In the case of the NTX 2500 tool spindle, the maximum oscillation frequency is 25 Hz. It is worth noting that LFV can only vibrate in one axis at a time, therefore, in some programs it may be beneficial to change the vibrational axis mid-program. In the initial case considered in this research, to rough the acetabular liner's outer hemisphere, the vibration was in the Z direction. The positive Z direction is denoted in Figure 3.

$$\text{Maximum oscillation frequency} = \frac{\text{RPM} \times I}{60} \quad (1)$$

Following the software retrofit, LFV can be turned on/off by the following addition to NC code:

```
G8.5 P2 Z0 I0.35 K1.2
```

```
NC code with LFV turned on ...
```

```
G8.5 P0
```

The NC code above defines the vibration direction (Z0), number of cycles per rotation (0.35) and amplitude magnification (1.2).

The representative workpiece was based on standard sizes for acetabular liners and to minimise material usage the smallest standard size was replicated (outer diameter of 42 mm and inner diameter of 28 mm). The experimental trials used medical grade GUR 1050 UHMWPE in a 50 mm diameter bar which was supplied by Orthoplastics.

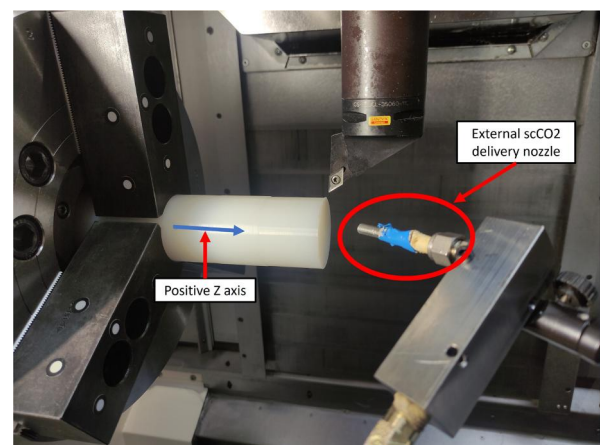


Figure 3. External scCO₂ nozzle directed at the front of the DCGX insert/UHMWPE bar.

The machining was split into four trials as summarised in Table 1. The first trial focused on the implementation of LFV to the machining of UHMWPE, for this trial, it was applied to the roughing of the outer hemisphere, due to this operation removing the greatest quantity of material and it being the first operation performed on the acetabular liners. Trial 2 used the optimised LFV parameters from Trial 1 to rough the acetabular liner's outer hemisphere and included compressed air or scCO₂. However, in Trial 3, solely scCO₂ without no LFV was used. The main machining trial, Trial 4, was split into two batches of acetabular liners, the first batch did not use LFV, whilst the second batch implemented LFV in all roughing operations. Note, it was planned to not use a coolant (scCO₂ or an air supply) in Trial 4 so that the impact solely from LFV could be seen on the manufacturing process. The primary focus of the machining trial was to reduce the quantity of swarf remaining on the acetabular liner after each operation. This would therefore, reduce the likelihood of the swarf impacting the machining process and eliminate the need for the machine tool operator to manually remove the swarf. To provide a comparison between the differing machining methodologies the mass of swarf remaining on the part (and tool) after the machining process was used. However, it should be noted that the quantity of swarf on the part (and tool) once the machining operation has finished is not necessarily the peak quantity of nested swarf and, therefore, the masses shown here should be considered as a lower bound of the swarf nests true mass.

Trials 1–3 (Table 1) focussed on the roughing of the outer hemisphere of the acetabular liner, and the insert for this operation was a Sandvik DCGX 11 T3 04-AL H10. A summary of the insert parameters is shown in Table 2.

In the trials using scCO₂ (Trials 2 and 3), the PureCut system [27] was used in its scCO₂ only mode, not scCO₂ mixed with minimum quantity lubricant. The scCO₂ was directed to the cutting zone by a single external nozzle that was directed at the insert, such as shown in Figure 3. The external scCO₂ delivery system features a 0.2 mm sapphire nozzle (Teschke WHD-shop, TN: 6202.0020.0). The flowrate for the trials was fixed at 15 kg/hr, this was done as it was the greatest flowrate achievable

Table 1. Stages of the UHMWPE machining trials.

Trial No.	Summary	No. of parts
1	LFV implementation and parameter optimisation	14
2	Optimised LFV with scCO ₂ or an air supply	3
3	scCO ₂ without LFV	3
4	Acetabular liner manufacture	27

Table 2. Parameters of a DCGX 11 T3 04-AL H10 insert.

Parameter	Value	Unit
Insert shape	D	–
Grade	H10	–
Corner radius	0.40	mm
Inscribed circle diameter	9.525	mm
Workpiece materials	N, S	–

with the selected nozzle and as trials were focused on varying the LFV parameters a binary on/off use of scCO₂ was deemed satisfactory.

To study the chip morphology a high-speed camera, the Photron FASTCAM Mini UX100, was used to record the cutting process at 3,200 frames per second with a shutter speed of 1/25600 sec and resolution of 640 × 320 pixels.

UHMWPE has a relatively low melting temperature of 130 °C [42–44] and the material properties vary significantly from room temperature to its melting temperature. Furthermore, UHMWPE has previously shown machinability benefits from cryogenic machining. However, the glass transition temperature differs significantly based on the source (–110 °C and –160 °C [11, 16, 20, 24] versus an outlier of –26 °C from Kustandi et al. [25]). Therefore, an in-depth understanding of the material properties of UHMWPE is required to identify the ideal cutting zone temperature of UHMWPE and to ascertain the glass transition temperature of the medical grade GUR 1050 used in the trials. To study the material properties a Perkin Elmer Differential Scanning Calorimetry (DSC) 4000 and Perkin Elmer Dynamic Mechanical Analysis (DMA) 800 were used.

The DSC study was conducted from –60 °C to 200 °C, ideally, the test would be to temperatures below –160 °C to be below the expected T_g . However, the lowest temperature achievable with the DSC 4000 was –60 °C; therefore, DSC testing was aimed to determine whether the outlier T_g proposed by Kustandi et al. [25] was representative of the GUR 1050 used in this trial. The UHMWPE samples were heated from –60 °C to 200 °C at a rate of 10 °C per minute including three repeats.

The DMA testing was performed using the Perkin Elmer DMA 8000 to measure the changes in rheological behaviour under dynamic loading as a function of temperature, time, frequency, stress, and atmosphere. The Perkin Elmer DMA 8000 was capable of room temperature testing up to 400 °C. However, the test was conducted up to 200 °C to be equivalent to the DSC testing and sufficiently beyond the melting temperature (130 °C [42–44]). The samples for DMA testing were 47.5 mm x 10 mm x 5 mm and were heated at a rate of 5 °C per minute under a dual cantilever loading at 10 N with a loading frequency of 1 Hz.

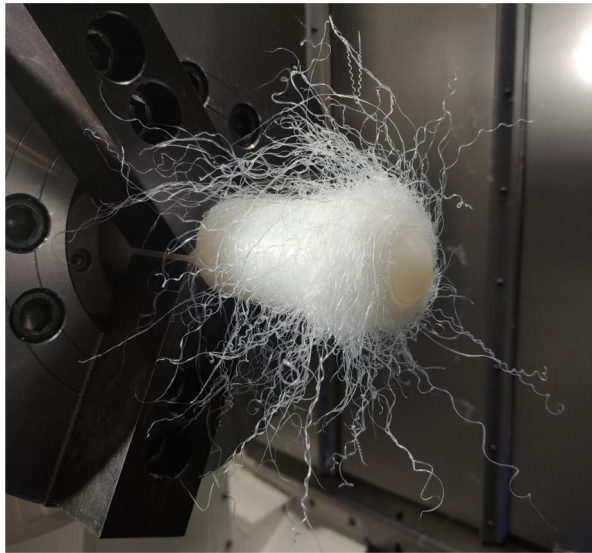


Figure 4. Post acetabular liner outer hemisphere roughing without LFV.

3. Results

3.1. Trial 1 – LFV optimisation

The first machining trial focussed on roughing the outer hemisphere of the acetabular liner. The hemisphere was initially roughed without using LFV, and this was done to highlight the current state of the standard industrial process of turning UHMWPE. The UHMWPE bar post-roughing a hemisphere without LFV is shown in [Figure 4](#).

The extent of the swarf nested around the bar in [Figure 4](#) prevents the geometry of the roughed acetabular liner hemisphere from being visible post-machining. The swarf nest was detached from, but, wrapped around the bar and had a mass of 7.5 g. For scale, the finished UHMWPE acetabular liner had a mass of 18.0 g. Furthermore, a significant amount of swarf (3.9 g) melted to the tip of the insert, shown in [Figure 5](#). The swarf melted to the insert which led to a deterioration in surface finish after the roughing operation and led to a greater amount of stock remaining on the component. The sheer quantity of swarf that was wrapped around the bar is shown in [Figure 6](#). In a standard industrial process when machining UHMWPE, this material is manually removed after each operation.

A series of hemispheres were roughed whilst varying the LFV parameters to visualise their impact on the chip morphology, a summary of these iterations is shown in [Table 3](#). The initial roughed hemisphere, without using LFV (shown in [Figure 4](#)) is also shown in [Table 3](#) as Iteration No. 1. The initial LFV parameters as shown in [Table 3](#) (Iteration No. 2) ($I = 0.35$, $K = 1.2$) were recommended by DMG Mori. Note that the feedrate was halved, as recommended when implementing LFV. The



Figure 5. UHMWPE swarf melted to the insert post hemisphere roughing.



Figure 6. Post acetabular liner outer hemisphere roughing without LFV swarf.

Table 3. Summary of chip readiness from varying LFV parameters. Note that K and I were previously defined in section 2.

Iteration No.	K	I	Feed rate (mm/rev)	Chip readiness	Repeat No.
1	–	–	0.1	Swarf not chipping	1
2	0.35	1.2	0.05	No observable change	1
3	0.35	2	0.05	No observable change	1
4	0.35	2	0.1	Sporadic chipping	1
5	0.5	2	0.1	Consistent chipping	9

parameters of each iteration were based on communication with DMG Mori and how the previous iteration performed.

In the initial implementation of LFV (Table 3 Iteration No. 2), the parameters suggested by DMG Mori, had no observable change in the swarf chip propensity. This was considered to be due to the amplitude of vibration being insufficient to instigate an air cut, and therefore, the swarf did not chip. Two sequential iterations were performed (Iteration No. 3 and 4) which increased the amplitude of vibration and feedrate respectively to increase the likelihood of making an aircut, this led to sporadic chipping of the UHMWPE. The fifth iteration increased the number of LFV cycles per rotation to 0.5, as the machining process was found to be unstable at 0.35 cycles per rotation. Increasing the cycles per rotation led to a more stable process whilst increasing the chip propensity. Iteration No. 5 had a rotational speed of 2500 rpm; therefore, the frequency of vibration was 20.8 Hz alongside an amplitude of 0.1 mm, and this amplitude is significantly greater than typically used for LFV but due to a polymer being machined, this was achievable without issue.

Overall, the addition of LFV to turning UHMWPE caused a drastic change in the chip morphology of the polymer. Application of the LFV parameters for Iteration No. 5 (Table 3) to the roughing of a hemisphere led to the hemisphere shown in Figure 7. Note that no swarf was removed before taking the image and the full profile of the component is visible, unlike the equivalent program without LFV (Figure 4). After Iteration No. 5, the LFV parameters were fixed, a further nine outer hemispheres were roughed, and the mean and standard deviation of the swarf remaining on the liner was $0.69\text{ g} \pm 0.62\text{ g}$. The chipped swarf consisted of tight curls of approximately 100 mm in length (Figure 8).

In Figure 7, the quantity of swarf remaining on the bar post roughing equated to several chips worth of UHMWPE (0.28 g compared to 7.5 g from Iteration No 1. Furthermore, the increase in chip propensity led to no swarf melting to the insert, therefore, leading to the geometry of the roughed hemisphere not being damaged by melted swarf. In previous research, an increase in the propensity of UHMWPE chipping was only seen from the cryogenic machining of the material. In the case of Aldwell et al. [17], the work identified a variation in chip type depending on the workpiece's initial temperature and the wear state of the tool. The research showed that the combination of workpiece cooling and a degraded tool changed the chip type from continuous to discontinuous through to dust. The workpiece in that case was chilled in a bath of liquid nitrogen for 24 h before machining. However, no temperature measurements were taken during the

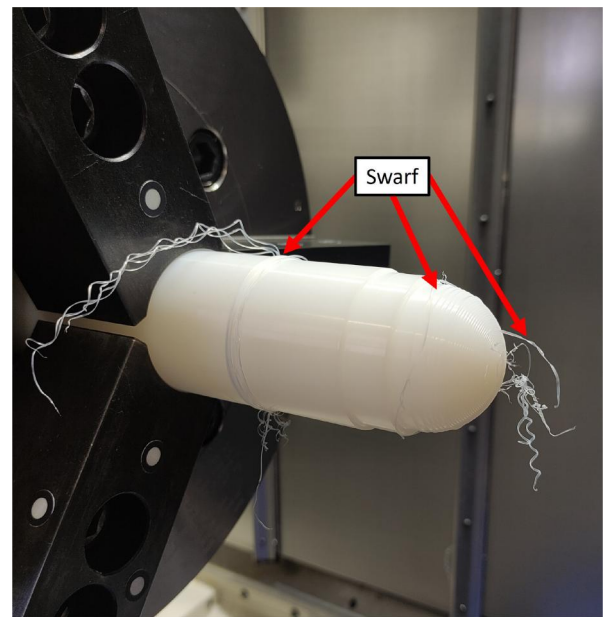


Figure 7. Post acetabular liner outer hemisphere roughing with LFV.



Figure 8. Post acetabular liner outer hemisphere roughing with LFV swarf.

machining; therefore, it is unknown how chilled the material was once it was in the machine tool or in the cutting zone itself. Overall, a change in chip type for UHMWPE machining from material cooling has previously been demonstrated, however, there may be considerable impracticalities when implementing cryogenic cooling in a production environment. Especially, if that cooling involves immersing the stock in a bath of liquid nitrogen for extended intervals. This highlights the potential benefits of LFV implementation, which has a significant improvement in chip morphology (beyond those from cryogenic cooling as UHMWPE dust chips are associated with a poor surface finish) from a software retrofit, whilst avoiding the requirement of material cooling.

To further understand the change in chip morphology a high-speed camera was used to study the roughing operation. Screenshots from the high-speed camera footage are shown in Figures 9–11, and the screenshots show progressive stages of the hemisphere roughing; second cut, tenth cut and near the centre of the hemisphere, respectively.

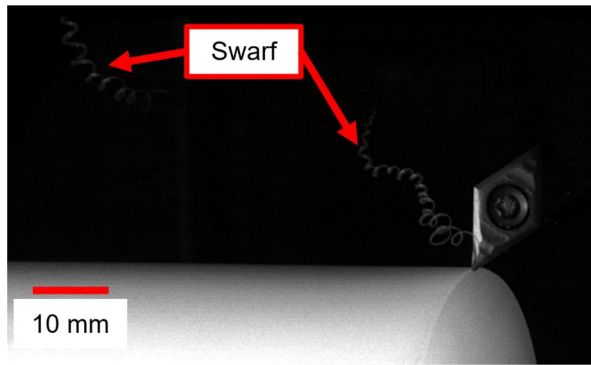


Figure 9. High-speed camera image of UHMWPE chipping whilst using LFV, showing the first pass second cut.

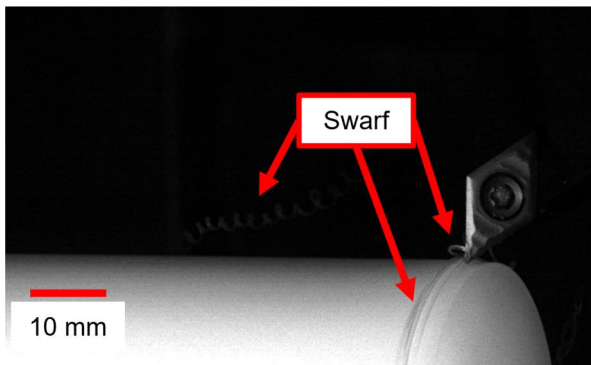


Figure 10. High-speed camera image of UHMWPE chipping whilst using LFV, showing the first pass tenth cut.

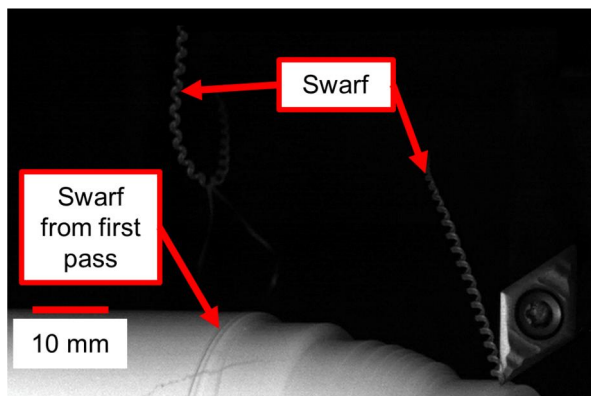


Figure 11. High-speed camera image of UHMWPE chipping whilst using LFV, near the Centre of the hemisphere.

The high-speed camera images (Figures 9–11) show a variation in the chip formation process across the roughing operation when using LFV and this sequence was repeated in sequential stages of the machining trials. During the first pass, the swarf was chipped (Figure 9) until a single cut did not chip (Figure 10), following this, the swarf began to wrap around the bar. This was only found to occur on the first pass down the length of the bar. Later cuts produced consistently chipping tight curled swarf (Figure 11), note the swarf from the first pass remaining on the bar in Figure 11. It is theorised that the medical grade UHMWPE has a variation in

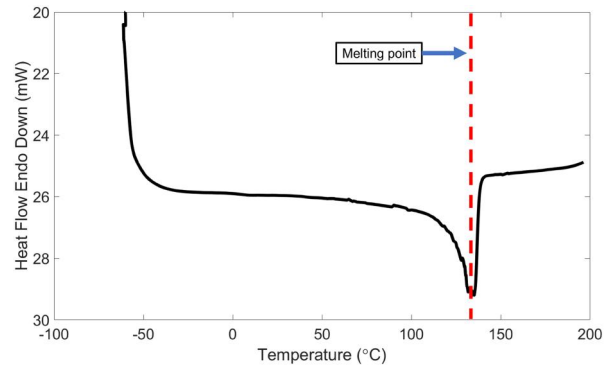


Figure 12. DSC test of GUR 1050 UHMWPE.

material properties at the surface, of an unknown thickness, but less than two depths of cut (1 mm), which impacts the propensity of the material to chip. The surface property variation of the UHMWPE is likely caused by the ram extrusion process to produce the bar stock. UHMWPE is a semi-crystalline polymer and the mechanical properties across the crystalline (polymer chains in highly orientated lamellae) and amorphous regions (polymer chains in a random orientation) vary [45] and, therefore, there may be a higher density of amorphous regions near the exterior of the ram extruded bar.

3.2. Trial 2 – LFV with a coolant

To ascertain how the properties of GUR 1050 change with temperature a DSC and DMA test was conducted using a Perkin Elmer DSC 4000 and Perkin Elmer DMA 8000, respectively. The results from the DSC test are shown in Figure 12.

The Perkin Elmer DSC 4000 used was only capable of temperatures down to -60°C . However, as there was minimal change in heat flow over the range -30°C to 60°C , it indicated that the glass transition temperature determined by Kustandi et al. [25] of -26°C was unrepresentative of the GUR 1050 used in these trials. Therefore, the glass transition temperature of the GUR 1050 used was assumed to be within the range -110°C and -160°C [11, 16, 20, 24]. This temperature range is sufficiently far from that achievable with a jet of scCO_2 and, therefore, all UHMWPE that was machined in this trial was in its ductile region.

The Perkin Elmer DMA 8000 was used to perform a DMA test on the GUR 1050 and the results from the testing are shown in Figure 13. The Perkin Elmer DMA 8000 used has no cooling capability; therefore, the results are presented as a comparison to those conducted by TA Instruments [46]. The testing by TA Instruments [46] ranged from -140°C to 100°C and provided an overlapping region (26°C – 100°C) to the DMA testing conducted on the Perkin Elmer DMA 8000. The work by TA

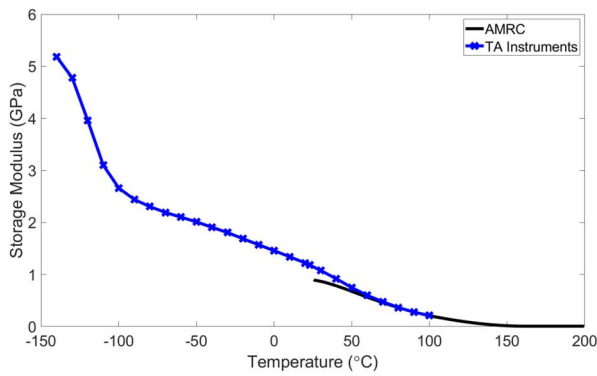


Figure 13. DMA test of GUR 1050 UHMWPE, the results are presented in comparison to those obtained by TA instruments [46].

Instruments conformed to the National Institute of Standards and Technology [47] SRM 8456 which identified the material as TICONA GUR 1050.

The region of Figure 13 covered by both tests (26°C – 100°C) indicated close conformance in the material property testing, especially above 50°C . For example, at 100°C the deviation between the two tests was less than 2%. The testing by TA Instruments [46] ranged from -140°C to 100°C , versus the DMA testing performed in this work which was from 26°C to 200°C . Due to the close alignment between the two tests, Figure 13 could be used as indicative of the storage modulus over the temperature range, -140°C to 200°C . In summary, the DSC and DMA testing shows the scale of UHMWPE property variation over relatively small temperature ranges when considering typical machining processes. Therefore, if a cryogenic coolant such as scCO₂ was used in the machining of UHMWPE, the temperature reduction (even though the temperature would remain above the T_g), would lead to significantly different material properties than when machined dry. For example, in Aldwell et al. [17], a temperature reduction led to a greater chip propensity. However, Figure 13 shows an approximately linear relationship between storage modulus and temperature from -100°C to 100°C . A general recommendation of a lower temperature (and thus greater storage modulus) may aid chip propensity, however, an ideal maximum temperature of the material is unknown and would require significant additional research. However, it is plausible that temperature consistency and, therefore, consistent material properties may be more desirable than a temperature reduction.

Based on the results from the DSC and DMA testing, LFV was combined with scCO₂ using the PureCut [27] system. In this stage of the machining trials, an external nozzle scCO₂ delivery system was used and two nozzle positions were considered; directed that the front of the DCGX insert/UHMWPE bar (Figure 3) and mounted to the tool

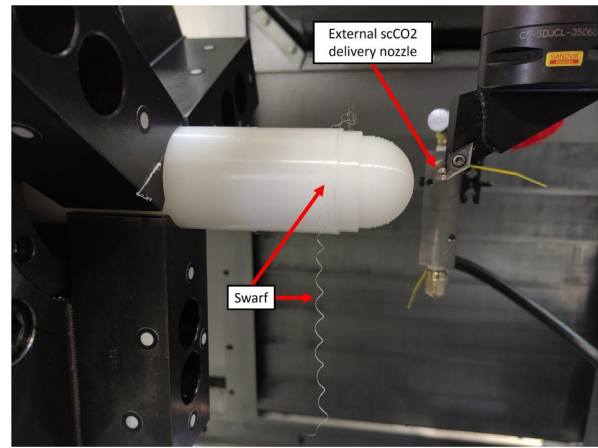


Figure 14. Post acetabular liner outer hemisphere roughing when using LFV with the addition of scCO₂.

spindle directed at the back of the DCGX insert (Figure 14). When the nozzle was mounted to the tool spindle it enabled the nozzle to move with respect to the tool. A typical acetabular liner hemisphere after the roughing operation when using LFV with the addition of scCO₂ is shown in Figure 14.

The addition of scCO₂ to the roughing program for the outer hemisphere (shown in Figure 14) further reduced the quantity of swarf remaining on the part post roughing to a single piece of swarf. For scale, this equated to 0.038 g of UHMWPE, relative to 7.5 g without LFV and $0.69\text{ g} \pm 0.62\text{ g}$ when using LFV without scCO₂. The remaining swarf was located beyond the part-off location, alleviating the potential for the swarf to impact the sequential machining programs. The trial shown in Figure 14 was repeated using compressed air instead of scCO₂ and the same swarf reduction was seen. Therefore, the swarf reduction is likely due to the fluid flow aiding chip detachment from the UHMWPE bar rather than a variation in chip morphology from a reduced UHMWPE temperature. The cryogenic coolant or air supply had no discernible impact on the chips formed, swarf like that previously seen in Figure 8 was produced. Furthermore, it was found that less swarf wrapped around the UHMWPE bar when using the scCO₂ directed at the front of the insert/bar (0.0119 g, Figure 14) than when directed at the back (0.0379 g, Figure 3) even though in the second setup, the nozzle moved with respect to the tool.

3.3. Trial 3 – coolant without LFV

The addition of a coolant (scCO₂ or compressed air) was shown to reduce the quantity of swarf remaining on the UHMWPE acetabular liner after the outer hemisphere was roughed. To identify the coolant's standalone impact on chip formation

the coolants were used without LFV. Images from the high-speed camera footage are shown in Figures 15–17 for the first pass and near the centre of the hemisphere. Note that images are only shown for scCO₂ as no variation between coolant type was observed.

The jet of scCO₂ had an identifiable build-up of frost on the insert/part highlighted by the colour change in Figure 15, which dissipated once the cutting process began, see Figure 16. The inability of UHMWPE to chip purely from the addition of scCO₂ is shown in Figure 17. Note that 9.79 g of swarf remained on the bar after the hemisphere was roughed, whereas in the LFV trial (Trial 1) the mean quantity of swarf remaining was $9.71 \text{ g} \pm 3.05 \text{ g}$. As the insert was not phasing between UHMWPE and air cutting, the swarf wrapped around the bar, ultimately leading to the scCO₂ being directed at the swarf instead of the cutting zone. Equivalent results were observed when using compressed air, therefore, a solution of a jet of high-velocity fluid directed at the insert is likely not



Figure 15. High-speed camera image of UHMWPE whilst using scCO₂, prior to the first cut.

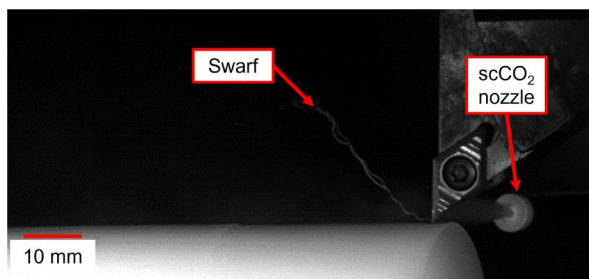


Figure 16. High-speed camera image of UHMWPE whilst using scCO₂, during the first pass.



Figure 17. High-speed camera image of UHMWPE whilst using scCO₂ near the centre of the hemisphere.

sufficient to chip the material. However, it has been demonstrated that LFV in combination with a jet of fluid directed at the insert provided benefits beyond those seen for LFV on its own, as the combination resulted in a further reduction in swarf remaining on the component. No potential benefit of scCO₂ over compressed air has been shown in these trials. However, it is plausible that the addition of scCO₂ may aid in preventing localised melting of UHMWPE in the cutting zone more than compressed air, as the melting temperature is between 125°C–150°C [42–44], although further research is required.

3.4. Trial 4 – acetabular liner manufacture

Following the LFV trials, a series of acetabular liners were manufactured with and without LFV (14 with LFV, 13 without LFV) to visualise the impact of LFV on the complete manufacturing process. When LFV was implemented, it was included in all roughing operations of machining an acetabular liner. To identify the impact solely from LFV, no scCO₂/compressed air was used in this trial. The same tooling suite was used for both manufacturing methodologies and the only modification to the toolpaths was the addition of the code to implement LFV.

Similar to what had been observed in Trial 1, the batch without LFV required the swarf to be manually removed after each roughing operation. Furthermore, in 6 of the 13 acetabular liners which did not use LFV, the swarf melted to the insert during the roughing of the outer hemisphere, damaging the surface of the roughed component. This would have likely led to the parts being scrapped in an industrial environment. When the acetabular liners were parted off and transferred to the sub-spindle the swarf was often caught between the sub-spindle jaws and the component leading to gouges in the finished liner. Conversely, when LFV was implemented into all roughing operations, minimal swarf remained on the roughed outer hemisphere and the swarf that remained was beyond where the component was parted off. This prevented the swarf from being trapped between the sub-spindle jaws and the acetabular liner. Furthermore, no swarf melted to any tool and no gouges were observed in any of the LFV batch. Similarly, no swarf was found to have melted to any tool during the LFV batch.

The UHMWPE liners produced were optically inspected using an Alicona G5. The measurements used a 50x magnification, Lambda-C of 80 μm and a sampling distance of 0.18 μm. The measurements were also performed in accordance with ISO 7206-2:2011. For clarity, the acetabular liners were inspected after the part was finished, even though

LFV was only used in the roughing operations, therefore, the inspected surfaces are not those left from LFV. As LFV was implemented into the roughing operations, this therefore prevented the potential for the roughing swarf to impact the surface finish of the finishing operations as well as removing the need for the machine operator to manually remove the swarf. Therefore, LFV has the potential for an indirect improvement in the completed component surface roughness relative to not implementing LFV.

ISO 7206-2:2011 defines an acceptable surface roughness (R_a) of the articulating surface of an acetabular liner as less than $2 \mu\text{m}$. Note that the ISO standard only refers to the surface roughness of the articulating surface and the standard follows the guidance outlined in ISO 4288:1996. Alicona measurements were taken on each acetabular liner and the measurements had a cut-off value of 0.8 mm , were taken at least 5 mm from the liner edges and approximately perpendicular to machining marks as outlined in the ISO standard. Furthermore, for conformance with the ISO standard, the mean R_a and standard deviation of the R_a are presented for both machining methodologies in Table 4 and Table 5, respectively.

Table 4 shows that the addition of LFV led to major reductions in the surface roughness on all surfaces measured, especially the outer hemisphere which had a 75% reduction in surface roughness and the standard deviation reduced by 83%. The smallest reduction was for the inner hemisphere which had a reduction of 53%. Note that the surface roughness values when LFV was used met the surface roughness requirement defined in ISO 7206-2:2011 and the batch without LFV did not. Similar trends were seen in the standard deviations (Table 5), with LFV leading to small variations in the surface roughness on each of the surfaces considered. The reduction in

Table 4. Mean R_a measurements on the representative acetabular liners manufactured.

Acetabular liner Manufacturing Methodology	Front face μm	Inner Hemisphere μm	Outer Hemisphere μm
Without LFV	2.15	2.30	3.37
With LFV	0.78	1.08	0.86
Percentage Reduction	64	53	75

Table 5. Standard deviation of the R_a measurements on the representative acetabular liners manufactured.

Acetabular liner Manufacturing Methodology	Front face μm	Inner Hemisphere μm	Outer Hemisphere μm
Without LFV	0.38	1.17	2.12
With LFV	0.35	0.30	0.36
Percentage Reduction	7.9	74	83

the mean and standard deviation of the surface roughness has the potential to reduce industrial scrap rates/amount of required rework of acetabular liners as the liners more readily meet the ISO standard.

4. Discussion

The general recommendation when implementing LFV is to halve the feedrate as the sinusoidal motion of the insert leads to the effective feedrate doubling during part of the cycle. This was followed in Trial 1, (see Iteration 1 in Table 3) when LFV was not implemented the machining program had a feedrate of 0.1 mm/rev whilst the sequential iterations had a feedrate of 0.05 mm/rev when LFV was included. However, it was found in the case of machining UHMWPE that the feedrate could increase back to its original value (0.1 mm/rev) without issue. This was likely due to a polymer being machined which is not associated with high machining forces. Therefore, it was possible to implement LFV with no loss of productivity. The only change to the NC code after including LFV was to reduce the spindle rotational speed (3000 rpm to 2500 rpm), this was because the NTX 2500 experienced a high-load error when LFV was combined with a rotational speed of 3000 rpm .

It is worth noting that the LFV trials shown in Trials 1–3 focus on the outer hemisphere roughing operation. However, the same benefits from LFV were seen in all roughing operations on the acetabular liner. This includes programs such as front face roughing or parting off which included LFV oscillating in the X direction (outer hemisphere roughing vibrated in the Z direction). For clarity, LFV should only be implemented into roughing operations, if it was added to finishing operations the surface finish would be significantly affected.

The quantity of swarf remaining on the UHMWPE bar after the outer hemisphere was roughed from the differing methodologies is summarised in Table 6.

Observation of Table 6 shows that the implementation of LFV led to a 91% reduction in the quantity of swarf that nested around the bar, as well as the prevention of swarf melting to the insert and damaging the component. However, when LFV was combined with a jet of high-velocity fluid directed at the

Table 6. The mean and standard deviation of the swarf nests from the varying machining methodologies.

Methodology	Swarf nest mean (g)	Swarf nest standard deviation
No LFV or coolant	9.72	3.05
LFV only	0.69	0.62
LFV and coolant	0.12	0.10
Coolant only	9.79	–

bar/insert a 98% reduction in the swarf nest was achieved. Therefore, a major reduction in swarf nesting can be attained from LFV; however, those benefits can be enhanced by a jet of fluid directed at the UHMWPE bar/insert. There could be even greater benefits from the scCO₂ if it was through-tool instead of from an external nozzle, this would aid in directing the scCO₂ to the cutting zone instead of cooling the bulk material. However, some machine tool suppliers are hesitant to implement through spindle scCO₂ due to the potential damage to seals etc.; therefore, solutions such as an Alberti Cryo Head [48] are viable routes for through tool scCO₂.

The improvements seen in the machinability of UHMWPE have significant potential benefits in industrial applications. Primarily, LFV alleviates the need for the machine operator to manually remove the swarf from the tool/component after each roughing operation. This enables a productivity improvement in the process, in this machining trial, a cycle time reduction of nearly 5% was achieved through removing the operator intervention. This also enables potential un-manned operation of the machine tool for acetabular liner production which may prove a requirement to meet the increased demand for total hip arthroplasty operations. In addition, the prevention of swarf wrapping around the bar and insert aids to prevent UHMWPE melting and, therefore, avoided damage to the component. The combination of these factors would likely lead to a reduction in UHMWPE acetabular liner scrap rates/rework rates whilst the productivity of the process was increased.

Furthermore, Cubillos et al. [6] assessed five acetabular liner manufacturers against ISO 7206-2:2011 and two of those manufacturers were found to not meet the surface roughness requirements set. This research has shown that LFV is a viable route for those manufacturers to meet this ISO standard requirement through an indirect improvement in the mean and variation in the surface roughness.

5. Conclusions

The application of low frequency vibration, an intermittent cutting process, has led to a significant improvement in the swarf chipping propensity of UHMWPE. This led to a major reduction in the swarf remaining on the bar post-machining (91% reduction relative to the traditional process) and reduced the likelihood of UHMWPE melting. This was achieved whilst the original feedrate was maintained, differing from the typical application of LFV which requires the feedrate to be halved. The benefits of LFV were enhanced when combined with a jet of fluid directed at the insert (both compressed

air and scCO₂ were considered) leading to minimal swarf remaining on the component (98% reduction relative to the traditional process). Two batches of representative UHMWPE acetabular liners were manufactured, one set included LFV in all roughing operations whilst the other followed a more traditional manufacturing process for the medical industry. The inclusion of LFV led to a reduction in surface roughness (minimum reduction was 53%) which met the surface roughness requirements for the articulating surface defined in ISO 7206-2:2011. This machinability improvement alleviated the need for the machine operator to remove the swarf after each roughing operation, raising productivity. This has been achieved whilst the surface roughness of the acetabular liners was reduced, likely reducing the scrap rate of UHMWPE acetabular liners.

Acknowledgements

The authors would like to thank DMG Mori, specifically, Ridhwan Muharram for their guidance in implementing LFV and Brett Beckham for operating the machine and his machining insight. For the purpose of open access, the author has applied a Creative Commons Attribution (CC BY) licence to any Author Accepted Manuscript version arising.

Authors' contributions

Jack Rooke: conceptualization of this study, data curation, formal analysis, investigation, methodology, visualisation, writing – original draft, writing – review and editing. Richard Bonnell: conceptualization of this study, funding acquisition, methodology, supervision, writing – review and editing. Emily Pickford: conceptualization of this study, funding acquisition, methodology, supervision. Adam Brown: supervision, funding acquisition, writing – review and editing. David Curtis: supervision, funding acquisition, writing – review and editing.

Disclosure statement

The authors report there are no competing interests to declare.

Funding

This work was supported by HVM Catapult funding provided by Innovate UK (project number 160109).

ORCID

Jack Rooke  <http://orcid.org/0000-0003-0720-7891>

Richard Bonnell  <http://orcid.org/0009-0003-6531-5169>

Emily Pickford  <http://orcid.org/0009-0008-5548-4723>

Adam Brown  <http://orcid.org/0009-0001-1175-7055>

David Curtis  <http://orcid.org/0000-0001-6402-6996>

Data availability statement

The data that support the findings of this study are available from the corresponding author, Jack Rooke, upon reasonable request.

References

- Ferguson RJ, Palmer AJ, Taylor A, et al. Hip replacement. *Lancet*. 2018;392(10158):1662–1671. doi: [10.1016/S0140-6736\(18\)31777-X](https://doi.org/10.1016/S0140-6736(18)31777-X).
- OECD. Health at a Glance 2021, OECD; 2021. doi: [10.1787/ae3016b9-en](https://doi.org/10.1787/ae3016b9-en).
- Shichman I, Roof M, Askew N, et al. Projections and epidemiology of primary hip and knee arthroplasty in medicare patients to 2040-2060. *JBJS Open Access*. 2023;8(1):1–7. doi: [10.2106/JBJS.OA.22.00112](https://doi.org/10.2106/JBJS.OA.22.00112).
- JRI Orthopaedics. JRI Orthopaedics; 2024 [cited 2024 Jun 11]. Available from: <https://www.jri-ltd.com/>.
- Lestari WD, Danaryanto AT, Nugroho A, et al. Wear property of machined ultra high molecular weight polyethylene (UHMWPE) acetabular liner product with CNC milling. *J Mech Eng Sci Technol*. 2021;5: 110–122. doi: [10.17977/um016v5i22021p110](https://doi.org/10.17977/um016v5i22021p110).
- Cubillos PO, Santos VO, Pizzolatti ALA, et al. Evaluation of surface finish and dimensional control of tribological metal-UHMWPE pair of commercially available hip implants. *J Arthroplas*. 2018;33:939–944. doi: [10.1016/j.arth.2017.10.032](https://doi.org/10.1016/j.arth.2017.10.032).
- Zaribaf FP. Medical-grade ultra-high molecular weight polyethylene: past, current and future. *Mater Sci Technol (UK)*. 2018;34(16):1940–1953. doi: [10.1080/02670836.2018.1469455](https://doi.org/10.1080/02670836.2018.1469455).
- Patel K, Chikkali SH, Sivaram S. Ultrahigh molecular weight polyethylene: catalysis, structure, properties, processing and applications. *Prog Polym Sci*. 2020; 109:101290. doi: [10.1016/j.progpolymsci.2020.101290](https://doi.org/10.1016/j.progpolymsci.2020.101290).
- Baxter RM, Steinbeck MJ, Tipper JL, et al. Comparison of periprosthetic tissue digestion methods for ultra-high molecular weight polyethylene wear debris extraction. *J Biomed Mater Res B Appl Biomater*. 2009;91(1):409–418. doi: [10.1002/jbm.b.31416](https://doi.org/10.1002/jbm.b.31416).
- Musib MK. A review of the history and role of UHMWPE as a component in total joint replacements. *IJBE*. 2012;1(1):6–10. <http://article.sapub.org/10.5923.j.ijbe.20110101.02.html> doi: [10.5923/j.ijbe.20110101.02](https://doi.org/10.5923/j.ijbe.20110101.02).
- Kurtz SM. UHMWPE biomaterials handbook. 2nd Edition. Academic Press; 2009. <https://linkinghub.elsevier.com/retrieve/pii/B9780123747211X00016>
- Oral E, Christensen SD, Malhi AS, et al. Wear resistance and mechanical properties of highly cross-linked, ultrahigh-molecular weight polyethylene doped with vitamin E. *J Arthroplasty*. 2006;21(4):580–591. doi: [10.1016/j.arth.2005.07.009](https://doi.org/10.1016/j.arth.2005.07.009).
- Tsukamoto R, Chen S, Asano T, et al. Improved wear performance with crosslinked UHMWPE and zirconia implants in knee simulation. *Acta Orthop*. 2006;77(3): 505–511. doi: [10.1080/17453670610046479](https://doi.org/10.1080/17453670610046479).
- Axinte D, Guo Y, Liao Z, et al. Machining of biocompatible materials—recent advances. *CIRP Ann*. 2019; 68(2):629–652. doi: [10.1016/j.cirp.2019.05.003](https://doi.org/10.1016/j.cirp.2019.05.003).
- Kobayashi A. Machining of plastics. New York: McGraw-Hill; 1967.
- Aldwell B, Hanley R, O'Donnell GE. Characterising the machining of biomedical grade polymers. *Proc Inst Mech Eng Part B J Eng Manufact*. 2014;228(10): 1237–1251. doi: [10.1177/0954405413514956](https://doi.org/10.1177/0954405413514956).
- Aldwell B, O'Mahony J, O'Donnell GE. The effect of workpiece cooling on the machining of biomedical grade polymers. *Procedia CIRP*. 2015;33:305–310. doi: [10.1016/j.procir.2015.06.058](https://doi.org/10.1016/j.procir.2015.06.058).
- Kakinuma Y, Kidani S, Aoyama T. Ultra-precision cryogenic machining of viscoelastic polymers. *CIRP Annals – Manufact Technol*. 2012;61(1):79–82. doi: [10.1016/j.cirp.2012.03.039](https://doi.org/10.1016/j.cirp.2012.03.039).
- Bertolini R, Ghiotti A, Bruschi S. Machinability of polyamide 6 under cryogenic cooling conditions. *Procedia Manuf*. 2020;48:419–427. doi: [10.1016/j.promfg.2020.05.064](https://doi.org/10.1016/j.promfg.2020.05.064).
- Bertolini R, Ghiotti A, Bruschi S. Cryogenic machining to enhance surface finish of a biomedical grade ultra-high-molecular weight polyethylene. 24th International Conference on Material Forming, Liège, Belgique. *Esaform 2021*. 2021. doi: [10.25518/esaform21.3749](https://doi.org/10.25518/esaform21.3749).
- Ghosh R, Knopf JA, Gibson DJ, et al. Cryogenic machining of polymeric biomaterials: an intraocular lens case study. *Medical Device Materials IV: Proceedings of the Materials and Processes for Medical Devices Conference 2007; 2008*. p. 54–64. doi: [10.1361/cp2007mpmd054](https://doi.org/10.1361/cp2007mpmd054).
- Kakinuma Y, Yasuda N, Aoyama T. Micromachining of soft polymer material applying cryogenic cooling. *JAMDSM*. 2008;2(4):560–569. http://www.jstage.jst.go.jp/article/jamdsm/2/4/2_4_560/_article doi: [10.1299/jamdsm.2.560](https://doi.org/10.1299/jamdsm.2.560).
- Tapoglou N, Makris C. Co2-assisted machining of biocompatible polymer materials. *Procedia Manuf*. 2020;51:801–805. doi: [10.1016/j.promfg.2020.10.112](https://doi.org/10.1016/j.promfg.2020.10.112).
- Kurtz SM. The UHMWPE handbook. Academic Press; 2004. <https://linkinghub.elsevier.com/retrieve/pii/B9780124298514X50001>
- Kustandi TS, Choo JH, Low HY, et al. Texturing of UHMWPE surface via nil for low friction and wear properties. *J Phys D: Appl Phys*. 2010;43(1):015301. doi: [10.1088/0022-3727/43/1/015301](https://doi.org/10.1088/0022-3727/43/1/015301).
- Takumi M. 2023. [accessed 4 Dec 2023]. Available from: <https://takumiprecision.com/medical/>.
- Fusion Coolant Systems. Pure-cut and pure-cut+: sustainable cooling and lubrication for modern machining; 2023 [accessed 24 October 2023]. Available from: <https://www.fusioncoolant.com/solutions/pure-cut>.
- British Plastics Federation, Machining of plastics. 2020 [accessed 29 Apr 2024]. Available from: https://www.bpf.co.uk/plastipedia/processes/Machining_of_Plastics.aspx.
- Nakamura S, Nakanishi K, Ohara K, et al. Tool design for low-frequency vibration cutting on surface property. *Front Manuf Technol*. 2023;2:1079127. doi: [10.3389/fmtec.2022.1079127](https://doi.org/10.3389/fmtec.2022.1079127).
- Miyake A, Kitakaze A, Katoh S, et al. Chip control in turning with synchronization of spindle rotation and feed motion vibration. *Precis Eng*. 2018;53:38–45. <https://www.sciencedirect.com/science/article/pii/S0141635918300941> doi: [10.1016/j.precisioneng.2018.02.012](https://doi.org/10.1016/j.precisioneng.2018.02.012).
- Sugihara T, Enomoto T, Osaka University. Ultra-low-frequency vibration assisted machining of ti-6al-4v alloy. *Int J Automat Technol*. 2016;10(4):647–653. doi: [10.20965/ijat.2016.p0647](https://doi.org/10.20965/ijat.2016.p0647).

32. Plastic Turned Parts, Plastic turned parts. 2022 [accessed 1 Aug 2022]. Available from: <http://www.plasticturnedparts.co.uk/>.
33. Sandvik. Sandvik coromant challenge; 2023 [accessed 10 Aug 2023]. Available from: <https://www.home.sandvik/en/campaigns/startup-challenge/challenge-1/>.
34. Alonso U, Goirigolzarri B, Ostra T, et al. Low frequency vibration assisted drilling of pc1000 polycarbonate. *Procedia Manuf.* 2019;41:407–414. <https://www.sciencedirect.com/science/article/pii/S2351978919311138> doi: 10.1016/j.promfg.2019.09.026.
35. Khanna N, Agrawal C, Pimenov DY, et al. Review on design and development of cryogenic machining setups for heat resistant alloys and composites. *J Manuf Process.* 2021;68:398–422. <https://linkinghub.elsevier.com/retrieve/pii/S1526612521003832> doi: 10.1016/j.jmapro.2021.05.053.
36. Shokrani A, Dhokia V, Muñoz-Escalona P, et al. State-of-the-art cryogenic machining and processing. *Int J Comput Integr Manuf.* 2013;26(7):616–648. doi: 10.1080/0951192X.2012.749531.
37. Sivarupan T, Bermingham M, Ng C-H, et al. A review of the use of cryogenic coolant during machining titanium alloys. *Sustain Mater Technol.* 2024;40:e00946. doi: 10.1016/j.susmat.2024.e00946.
38. Sutherland JW, Richter JS, Hutchins MJ, et al. The role of manufacturing in affecting the social dimension of sustainability. *CIRP Ann.* 2016;65(2):689–712. <https://www.sciencedirect.com/science/article/pii/S0007850616301901> doi: 10.1016/j.cirp.2016.05.003.
39. Lu T, Kudaravalli R, Georgiou G. Cryogenic machining through the spindle and tool for improved machining process performance and sustainability: pt. i, system design. *Procedia Manuf.* 2018;21:266–272. <https://www.sciencedirect.com/science/article/pii/S2351978918301550> doi: 10.1016/j.promfg.2018.02.120.
40. Dhokia VG, Newman ST, Crabtree P, et al. A methodology for the determination of foamed polymer contraction rates as a result of cryogenic CNC machining. *Rob Comput Integr Manuf.* 2010;26(6):665–670. doi: 10.1016/j.rcim.2010.08.003.
41. Proud L, Tapoglou N, Slatter T. A review of CO₂ coolants for sustainable machining. *Metals.* 2022;12(2):283. doi: 10.3390/met12020283.
42. Miao W, Zhu H, Duan T, et al. High-density polyethylene crystals with double melting peaks induced by ultra-high-molecular-weight polyethylene fibre. *R Soc Open Sci.* 2018;5(7):180394. doi: 10.1098/rsos.180394.
43. Zhang H, Liang Y. Extrusion processing of ultra-high molecular weight polyethylene. InTech; 2018. <http://www.intechopen.com/books/extrusion-of-metals-polymers-and-food-products/extrusion-processing-of-ultra-high-molecular-weight-polyethylene>.
44. Tam T, Bhatnagar A. High-performance ballistic fibers and tapes. Elsevier. 2016:1–39. <https://linkinghub.elsevier.com/retrieve/pii/B9780081004067000015>
45. Sobieraj M, Rimnac C. Ultra high molecular weight polyethylene: mechanics, morphology, and clinical behavior. *J Mech Behav Biomed Mater.* 2009;2(5):433–443. doi: 10.1016/j.jmbbm.2008.12.006.
46. Blaine R. Weight polyethylene as a reference material for dynamic mechanical analysis NIST SRM 8456 ultra-high molecular; 2005.
47. Eichmiller F, Test J, Croarkin C. Mechanical properties of ultra high molecular weight polyethylene NIST reference material RM 8456; 2001 [accessed 10 July 2024]. Available from: https://tsapps.nist.gov/publication/get_pdf.cfm?pub_id=851782.
48. MAQcenter. Cryo Heads; 2024 [accessed 09 May 2024]. Available from: <https://maqcenter.com/producto/cryo-heads/>.